UNITED STATES DEPARTMENT OF THE INTERIOR

GEOLOGICAL SURVEY

Mineralogy and chemistry of ocean floor hydrothermal precipitates from Kolbeinsey and Reykjanes Ridges near Iceland: Scanning electron microscope (energy-dispersive X-ray) analysis

by

Robert F. Commeau[1]
Geoffrey Thompson[2]
Frank T. Manheim[1]
Jon Olafsson[3]
and
Sveinn P. Jakobsson[4]

Open-File Report 89-480

[1] U.S. Geological Survey, Woods Hole MA 02543
[2] Woods Hole Oceanographic Institution, Woods Hole MA 02543
[3] Marine Research Institute, Skulagata 4, 121 Reykjavik, Iceland
[4] Natural History Museum, P. O. Box 5320, 125 Reykjavik, Iceland

1989

INDEX MAP OF STUDY AREA

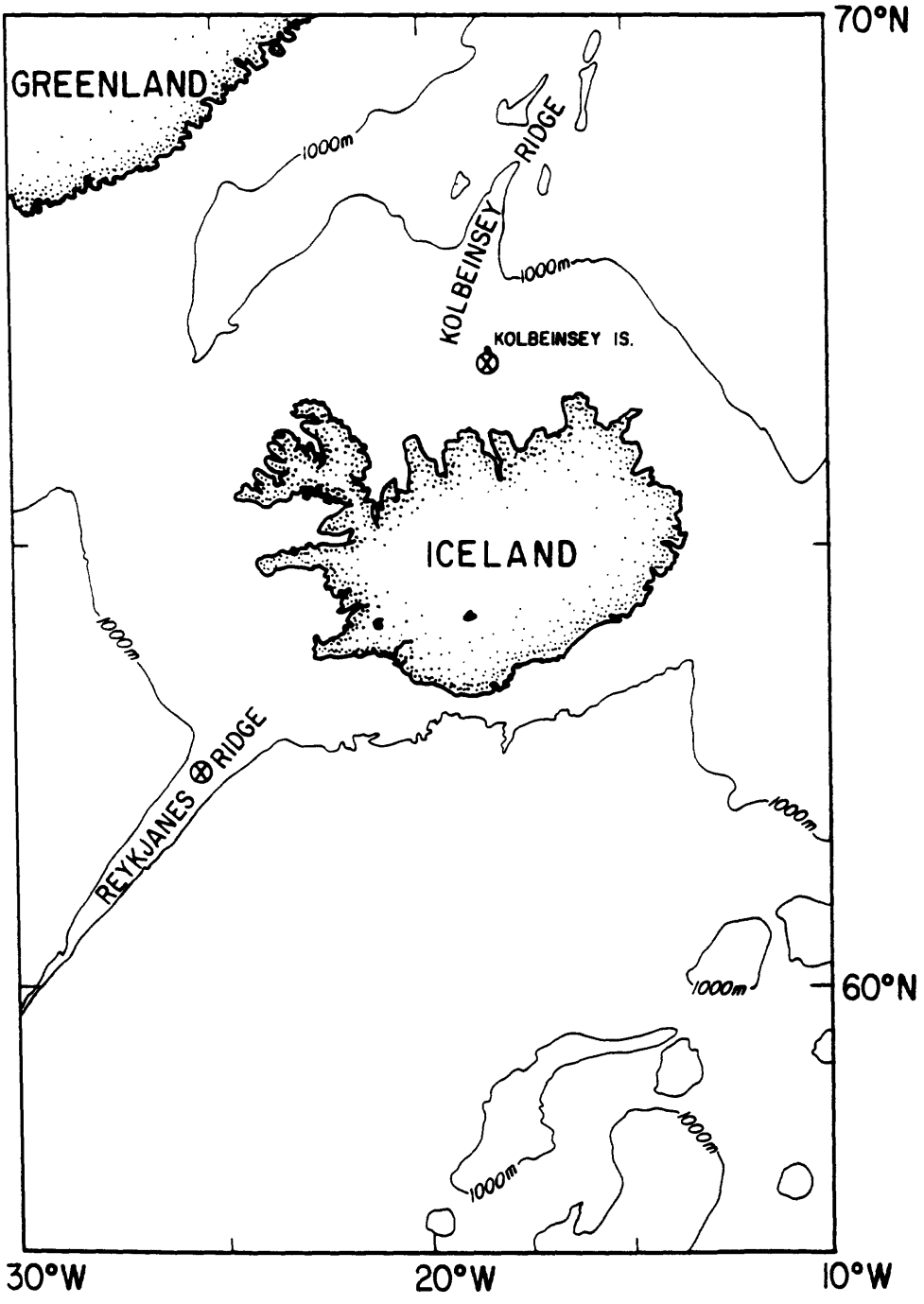

Dredge samples retrieved from locations marked with a circled X.

I INTRODUCTION

This report describes the mineralogy and associated chemistry of ocean floor mineral precipitates recovered from areas of hydrothermal emission on Kolbeinsey and Reykjanes Ridges which are located along the northern extension of the Mid-Atlantic Ridge near Iceland. Selected samples were examined in the scanning electron microscope (SEM) and analyzed using the energy-dispersive spectrometer (EDS) system.

The Kolbeinsey Ridge samples were dredged in June 1987 from an area of active hydrothermal emission. The site is 90 to 100 m deep, 110 km north of Iceland, and 6.6 km south of the island of Kolbeinsey (location marked on Index Map). The hydrothermal zone is located on a constructional volcanic edifice that is composed of tholeiitic basalts. The center of hydrothermal activity is denoted by boiling undersea springs emitting waters at temperatures of about 200 to 300 ^{0}C, rising gas bubbles, and sub-boiling seeps. A dense bacterial mat (Beggiatoa community) covers most of the site along with colonies of tunicates and the hydroid Cormorpha. The dredge sample (B6/87-326) recovered mainly volcanic rocks, including some breccia samples (inventoried as rock group 3) imbedded in hydrothermal precipitates. The breccia is composed of volcanic clasts of fine-grained vesicular basalt cemented with hyaloclastite, glass shards, and basaltic debris. The basalt is similar in mineralogy to the described sample 2677 (J. Olafsson and others, manuscript in preparation, 1989) with extensive alteration of glass and olivine, and replacement by clays and opaline silica. The breccia is embedded in a matrix of gypsum and barite with minor quartz, aragonite and basaltic debris. Filaments of bacterial mat cover the surface. Sulfide minerals are not abundant but are present as fine granules in the matrix and as infillings or linings in small cavities and vesicles in the basaltic clasts. Based on optical and x-ray diffraction studies, the sulfide minerals include major amounts of pyrite, minor amounts of marcasite and sphalerite, and trace amounts of cubanite, covellite, and bornite. This assemblage of sulfide minerals in association with Ca and Ba sulfates and silica is typical of many deep ocean vents and indicates that the breccia is in contact with relatively high temperature hydrothermal solutions. This report includes a descriptive study of the pyrite, silica, gypsum, barite, and smectite contained in sample B6/87-326.

Manganese-rich precipitations were dredged from Reykjanes Ridge by local fishermen at approximately 62^{0}27'N, 25^{0}26'W from a depth of 662 m in 1987 (location marked on Index Map). The Ridge, an extension of the south Iceland seismic zone, trends southwest, crossing a deep basement scarp delineating the Iceland Block (Saemundsson, 1986). From vesicularity studies of basalts on the ridge Duffield (1978) interpreted that original water depths decreased from 2700 m at 35.5 Ma to 700 m at 2.7 Ma. The ridge is an intensely active seismic feature (Einarsson, 1986) and the presence of fresh, glassy basalts (P. Meyer, oral commun., 1989) suggests that lavas younger than those mentioned above are likely. Contemporary hydrothermal venting may occur. The samples characterized in this report are predominately manganese oxide in the form of todorokite. The external morphology

is similar to hydrothermal manganese oxide precipitates recovered elsewhere along the Mid-Atlantic Ridge (Thompson and others, 1985; 1988; Lalou and others, 1988).

II MATERIALS AND METHODS

Samples

Rock samples collected from Kolbeinsey and Reykjanes Ridges are stored in depositories located at the Icelandic Museum of Natural History and the Marine Research Institute in Reykjavik, Iceland. Samples containing hydrothermal materials were submitted for examination at the laboratories of the Woods Hole Oceanographic Institution and the U.S. Geological Survey in Woods Hole, Massachusetts. In Woods Hole, mineral matter and organic material were removed from the rock samples and placed into vials for examination by optical microscopy, electron microscopy, and x-ray diffraction. Before the SEM/EDS study, the samples in the vials were inspected under the binocular microscope and a limited number were selected for analysis. The following list and brief description accompanied the material selected for SEM/EDS analysis.

Kolbeinsey Ridge

Vial No.	Description
3	Yellow "pyritic" crystals in cavity
5	Outer, loose granules including sulfides
7	Brown grains (wet vial)

Reykjanes Ridge

Vial	Description
A	Outer rind
D	Multilayered, crystalline inner portion

Sample Preparation

The samples were prepared first for quantitative energy-dispersive x-ray analysis. All samples were mounted on double-backed cellophane tape placed on aluminum SEM stubs. The double-backed tape chosen gives no spectral artifacts (elemental peaks coming from the tape or from the aluminum stub below it). Before mounting, the sample removed from vial A, Reykjanes Ridge, was ultrasonically cleaned in ethanol to remove the black-brown powder coating it.

The edges and, where possible, the underside of the samples were painted

with carbon cement to provide an electrically conducting path to ground. The mounted samples were then carbon-coated in the vacuum evaporator. After the x-ray analyses were performed, the samples were sputter-coated with gold-palladium before electron micrographs were taken.

Equipment

- ETEC, Model U-1 Scanning Electron Microscope (SEM)
- Kevex Corporation, 7000 Series Energy-dispersive X-ray Analyzer (EDS)
- Denton Vacuum Inc., Model DV-515 Vacuum Evaporator with sputter attachment
- Philips Electronic Instruments Inc., X-ray Diffractometer (XRD)

Electron Micrographs

Electron micrographs were taken at 20 keV (beam acceleration potential). Most of the photos shown in the figures are secondary electron micrographs. Two backscattered electron micrographs were taken on the sample from Kolbeinsey Ridge (vial no. 3; Figure 1j,l). A micron marker is on the first line of the script in the lower left hand corner of the photo (for example, "100.0 u l---l" means the distance of 100 microns between the "uprights" of the "H").

X-ray analysis

A. Principles

The USGS energy-dispersive spectrometry system uses a lithium-drifted silicon detector with a conventional beryllium window design. The detector can register x-rays from elements that have atomic numbers equal to or greater than that of sodium (At. No. 11). The ETEC SEM does not have a "Faraday cup" system with which to monitor a beam reference current. X-ray data collected from elemental and mineral standards are normalized to zinc K alpha counts and stored on computer disk. However, the zinc reference standard cannot be conveniently used when examining samples under the SEM. Our routine procedure for quantitative analysis is to analyze all elements (x-ray peaks) that the detector can "see". If appropriate, the elemental concentrations are converted to oxide concentrations to obtain oxygen via stoichiometry. The results are normalized to 100 percent (e.g., element concentrations in the case of pyrite and oxide concentrations in the case of barite).

Unlike samples prepared for conventional microprobe analysis, the samples prepared for SEM/EDS analysis were not polished in order to view and photograph them in a setting as close to natural as possible. Therefore

the x-ray take-off angle is not precisely known. Uncertainties in the x-ray absorption pathlength that result from this can have a major effect on the matrix correction routine and ultimately, the results. However this effect is minimized at high takeoff angles. The samples are manipulated in the SEM so that a high (but imprecisely known) takeoff angle is achieved. Typically, concentrations are accurate to plus or minus 2 to 5 percent of the amount determined in cases where all elements present are analyzed (R. F. Commeau, unpublished data, 1989). In cases where all components (e.g., H_2O) cannot be analyzed, the concentration values are too high because of the normalization technique employed. However, the concentration ratios are accurate to 3 to 7 percent.

B. Qualitative and Quantitative Analysis

X-ray spectra were acquired for qualitative and quantitative analysis for 100 seconds (live time) using a beam acceleration potential of 20 keV and approximately 150 pico-amps of beam current. The takeoff angle is approximately 53 degrees.

Photographs were taken of x-ray spectra collected from the samples (Figures 1-5). The peaks of interest have been labeled (according to element) and painted white. In general, all peaks labeled are K alpha lines. The only exceptions are the Sr and Ba (L alpha lines) in the two barite spectra (Figures 2c and 3c).

Many of the spectra collected were computer-processed to (1) remove the silicon escape peak, (2) remove the x-ray continuum or background, (3) deconvolute overlapping peaks, (4) integrate counts under the peaks, and (5) calculate element or element oxide concentrations using stored standards and a matrix correction routine (Colby, 1968) for atomic number, absorption, and fluorescence effects. The quantitative results have been tabulated and included with each sample description.

III SAMPLE DESCRIPTIONS AND SEM/EDS RESULTS

Vial No. 3, Kolbeinsey Ridge

There was only one grain in the vial (Figure 1a). Under the binocular scope the grain consists of a snowy white mineral growth at one end and shiny, silver-colored (metallic luster) mineral growth at the other. SEM/EDS examination revealed that the snowy white mineral is Si-rich and is inferred to be SiO_2, or silica (Figure 1b-h). Some of the broken surfaces show conchoidal fracturing (Figure 1h).

EDS analysis of the silver-colored grains matches the stoichiometry of pyrite (Figure 1i-m; Table 1). The silica growth coats the pyrite grains (Figure 1i-l) and to some degree protects the pyrite from chemical attack (oxidation). The original description submitted with this sample cited "yellow pyritic crystals". The yellow color is probably caused by partial oxidation of the iron in the outer surfaces of the pyrite. The pyrite in this sample is exposed along a fresh fracture surface and has not been oxidized, explaining the shiny silver color.

A sulfate mineral was observed in the form of clusters of radiating, bladed crystals growing on the surfaces of both the pyrite grains (Figure 1n) and the SiO_2 mineral (Figure 1d). EDS analysis revealed that the crystals contain Na, Ca, and S (Figure 1o; Table 2). It is an evaporite mineral in the Na-Ca sulfate series. A mineral called glauberite, $CaNa_2(SO_4)_2$, is similar in composition, but the EDS analysis in Table 2 doesn't quite fit its stoichiometry. The crystals are growing on fresh, fractured surfaces and probably formed as the sample dried.

Figure 1: Grain sample from vial no. 3, Kolbeinsey Ridge; SEM micrographs and EDS spectra.

a - Silica/pyrite grain; botryoidal silica above dashed line; silica-coated pyrite (fractured surfaces) below dashed line.
b - Botryoidal silica growth.
c - Close-up of botryoids and broken surface from center of 1b.
d - Silica growth; twin pyrite crystals (P) in lower left; Na-Ca sulfate crystals (S) on silica in lower right.
e - EDS spectrum of silica.
f - Close-up of botryoidal cluster from upper right of 1d.
g - Close-up of surface of botryoid from right center of 1f.
h - Conchoidal fracturing; broken silica surface.
i - Broken surface; silica covering pyrite; secondary electron image.
j - Same area as 1i; backscattered electron image.
k - Broken surface; silica covering pyrite; secondary electron image.

l - Same area as 1k; backscattered electron image.
m - EDS spectrum of pyrite grain no. 5 in Table 1.
n - Radiating, bladed crystals of Na-Ca sulfate sitting on pyrite; silica coating across top of picture.
o - EDS spectrum of bladed crystals on pyrite; results in Table 2.

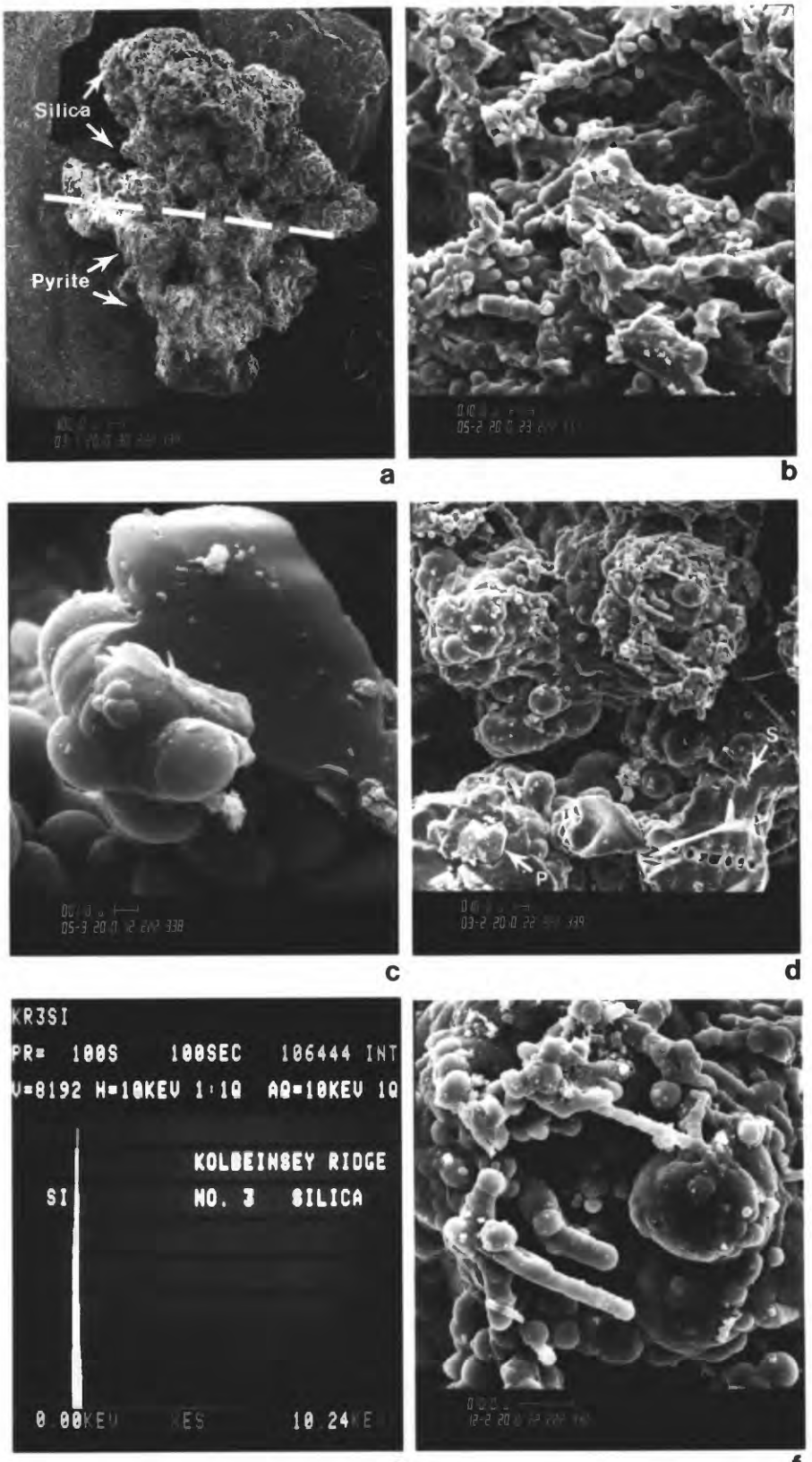
Silica
Pyrite
a
b
c
S
P
d
KR3SI
PR= 100S 100SEC 106444 INT
V=8192 H=10KEV 1:1Q AQ=10KEV 1Q
KOLBEINSEY RIDGE
NO. 3 SILICA
SI
0 00KEV
10.24KE
e
f

Figure 1

1a

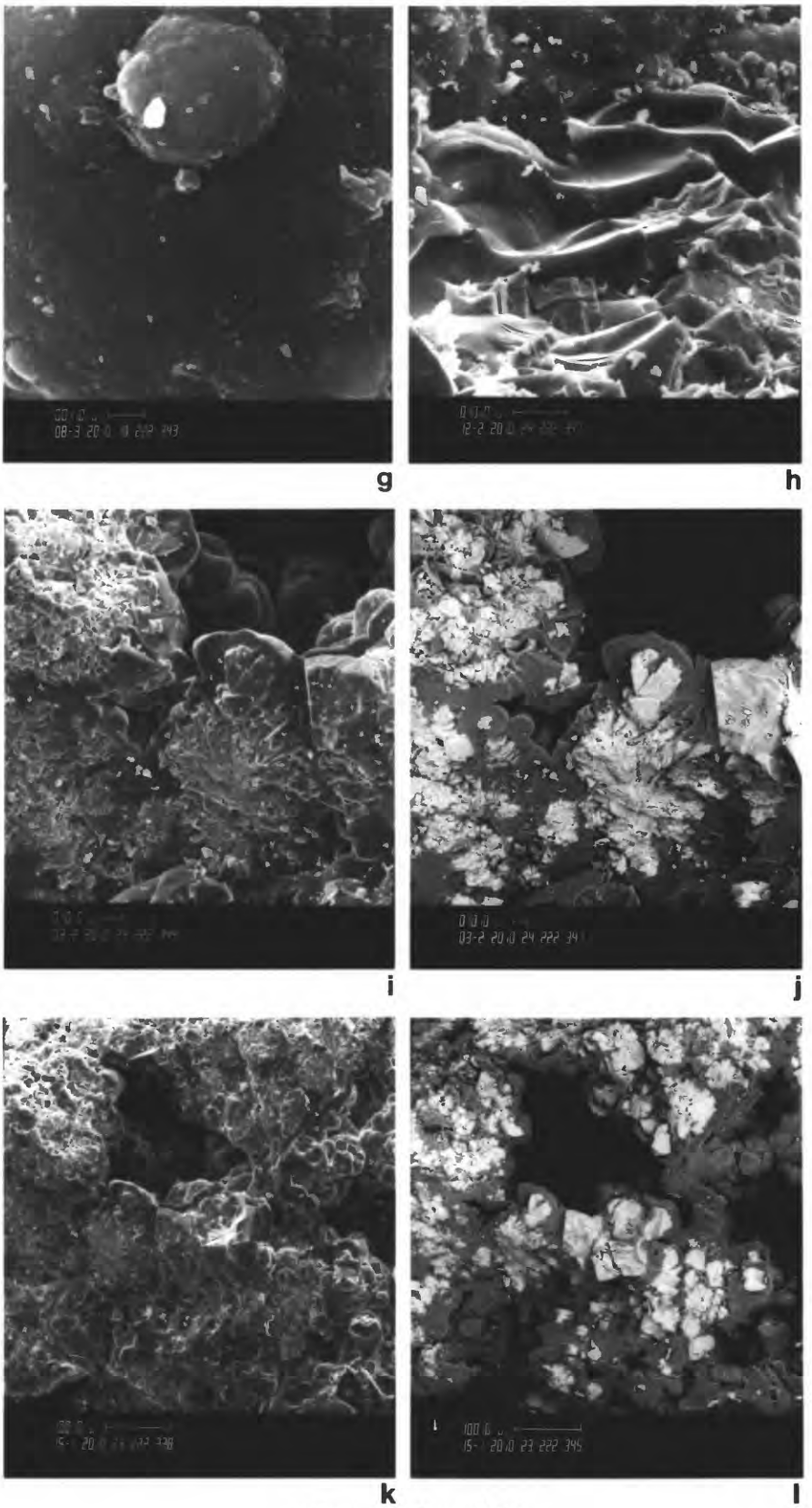

Figure 1 (cont'd)

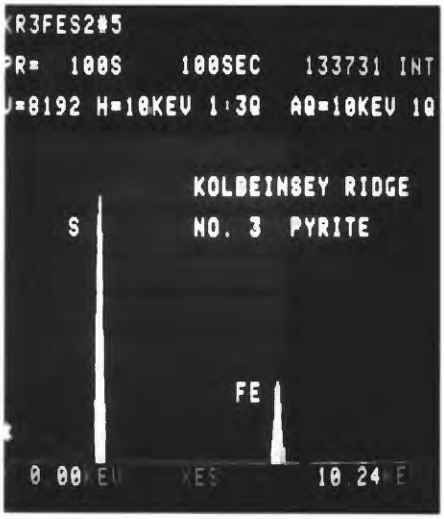

m

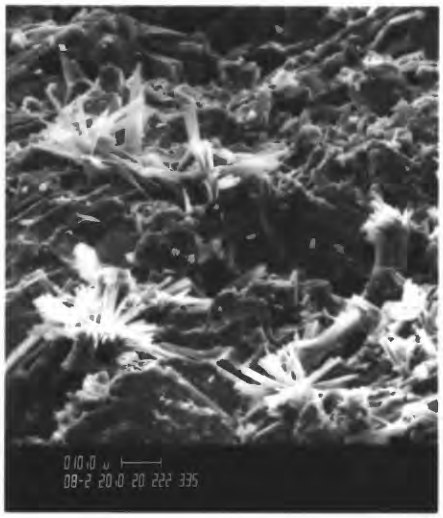

n

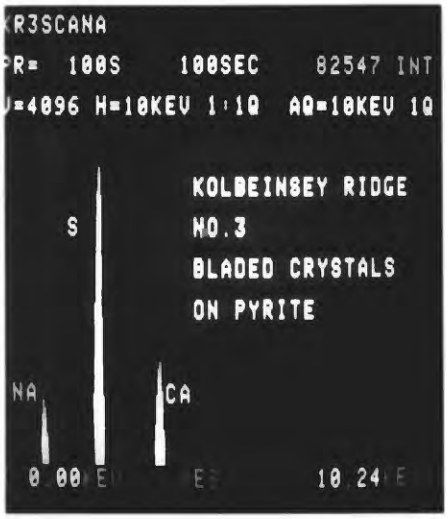

o

Figure 1 (cont'd)

Analyses of pyrite grains (in Wt. Percent):

Element	Grain No. 1	Grain No. 2	Grain No. 3	Grain No. 4	Grain No. 5	Mean	Stand. Dev. (n-1)	Theoretical Composition of Pyrite
S	54.08	53.08	54.33	52.69	52.94	53.42	0.72	53.45
Fe	45.92	46.92	45.67	47.31	47.06	46.58	0.73	46.55
Total	100.00	100.00	100.00	100.00	100.00	100.00		100.00

Table 1. Kolbeinsey Ridge, vial no. 3; analysis of five pyrite grains. The mean of the five analyses is close to the theoretical composition of pyrite. The standard deviations listed indicate the degree of accuracy that can be expected.

EDS output:

Element	Wt. %	Precision 2 Sigma	El. Oxide	Wt. %
Na	16.84	0.47	Na_2O	22.70
S	24.16	0.24	SO_3	60.33
Ca	10.41	0.19	CaO	14.57
Fe	1.68	0.14	Fe_2O_3	2.40
O *	46.91			
Total	100.00			100.00

Data after removing Fe and S attributed to pyrite:

Element	Wt. %	El. Oxide	Wt. %
Na	18.15	Na_2O	24.47
S	23.96	SO_3	59.83
Ca	11.22	CaO	15.70
O *	46.67		
Total	100.00		100.00

* Determined by stoichiometry

Table 2. Kolbeinsey Ridge, vial no. 3; analysis of radiating, bladed crystals of Na-Ca sulfate growing on pyrite. The first set of data is a copy of the output from the EDS unit. The second set lists the data after mathematically removing the Fe (Fe_2O_3) and a corresponding amount of S (SO_3) attributed to pyrite.

Vial No. 5, Kolbeinsey Ridge

Two samples were selected from vial no. 5. Under the binocular microscope, Sample A consists of a fine-grained aggregate of white crystalline material. The white matrix is flecked with fine, dark crystal grains. An SEM micrograph of sample A is shown in Figure 2a. SEM examination revealed that much of the white matrix consists of the botryoidal silica growths that have been documented in the sample from vial no. 3. Some of the white mineral material is halite, which precipitated during sample drying. The dark flecks are isolated clusters or individual grains of pyrite. Micrographs of the silica and pyrite were not taken because similar forms have been documented elsewhere. The sample did contain barite which contains some Sr (see Figure 2b,c). However, the barite was not a good candidate for quantitative analysis because it is covered with a thin layer of SiO_2. (A barite grain has been analyzed in a sample from vial no. 7, Figure 3b.)

Sample B, which appears to be of organic origin, is encrusted with mineral growth (Figure 2d-f). Under the binocular scope, the encrustation varies in color (patchy) from areas that are black with white flecks to areas that are white with black flecks. In the SEM many of the black areas were determined to be ferromanganese (Figure 2d); some of the black flecks are pyrite (Figure 2g). Much of the white-colored mineralization is Ca sulfate, probably gypsum (Figure 2g,h; Table 3). Other light-colored minerals found are silica (the botryoidal SiO_2 growths) and halite. The upper right corner of Figure 2g shows an area that is free of mineral growth. X-ray analysis of this area does not show any characteristic elemental peaks, which is typical for organic material.

Figure 2: Two samples from Kolbeinsey Ridge, vial no. 5; SEM micrographs and EDS spectra.

Sample A:

a - Botryoidal silica growth; area containing barite crystals (B) circled.
b - Barite rosette (circled in 2a) coated with silica; pyrite crystals (P) on the barite; rosette surrounded by silica.
c - EDS spectrum of barite in 2b.

Sample B:

d - Branched organic particle encrusted with minerals; ferromanganese (F) and gypsum (G).
e - Organic particle encrusted with minerals.
f - Enlargement, center of 2e; gypsum encrustation.
g - Center of Figure 2f, gypsum groundmass covered with smaller particles

and crystals of pyrite, halite, and silica; two pyrite crystals (P) lower left, organic substrate (O) upper right.

h – EDS spectrum of gypsum in 2g; results in Table 3.

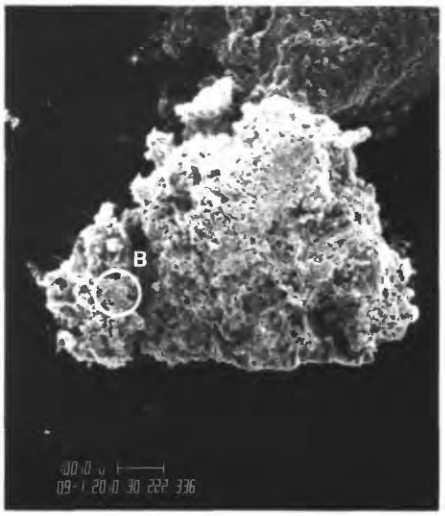

a

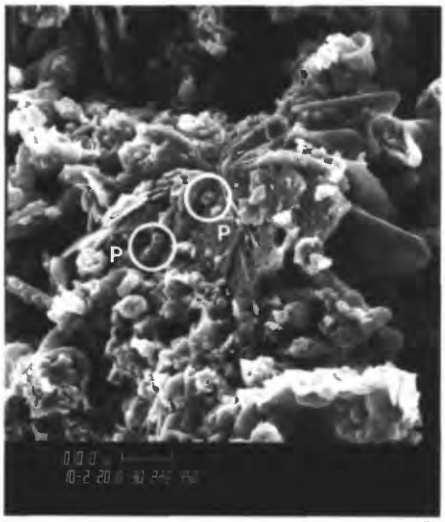

b

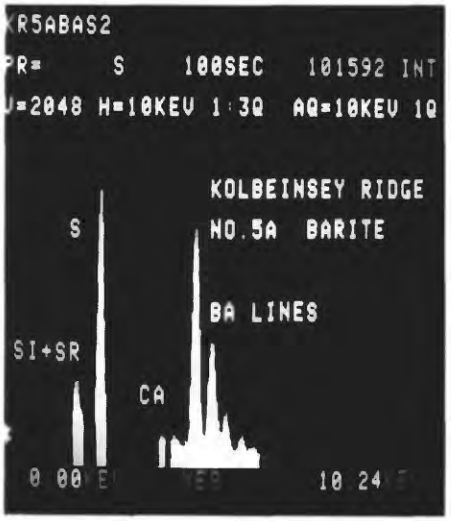

c

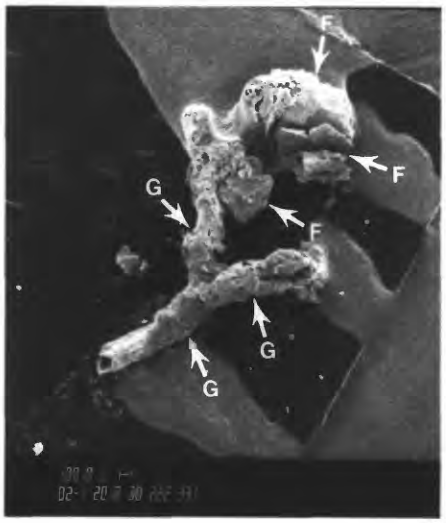

d

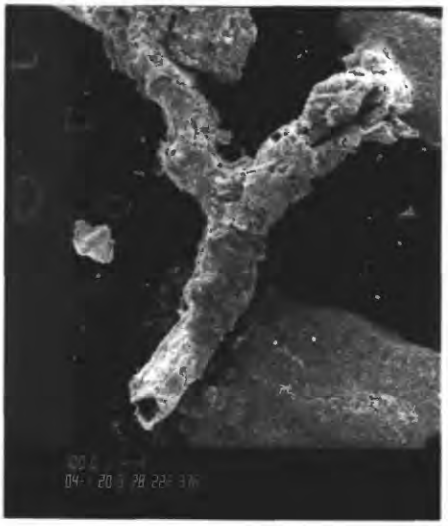

e

Figure 2

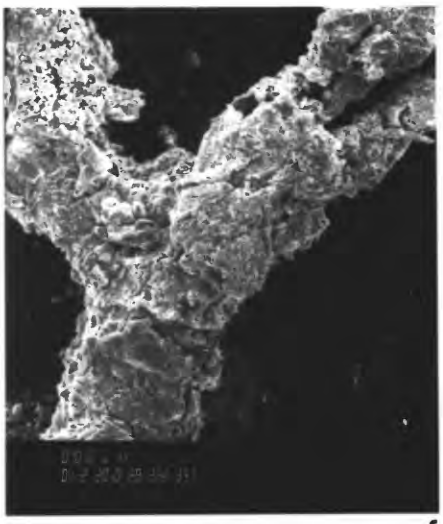

f

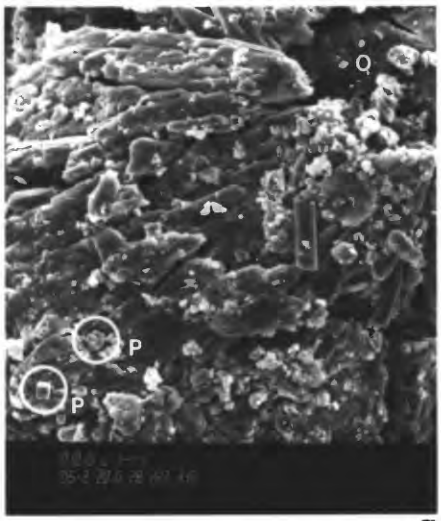

g

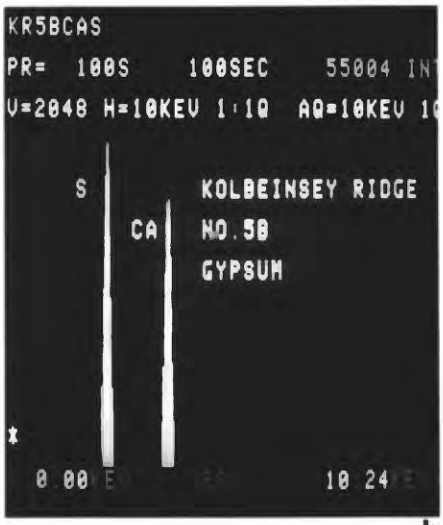

h

Figure 2 (cont'd)

EDS output:

Element	Wt. %	Precision 2 Sigma	El. Oxide	Wt. %
S	23.89	0.28	SO_3	59.65
Ca	28.84	0.37	CaO	40.35
O *	47.27			
Total	100.00			100.00

Data renormalized to include crystalline water:

Element	Wt. %	El. Oxide	Wt. %	Theoretical Composition of Gypsum (in Ox. Wt. %)
H	2.34	H_2O^+	20.93	20.93
S	18.89	SO_3	47.17	46.50
Ca	22.80	CaO	31.90	32.57
O *	55.97			
Total	100.00		100.00	100.00

* Determined by stoichiometry

Table 3. Kolbeinsey Ridge vial no. 5; analysis of gypsum in Sample B (Figure 2g and 2h). The first set of data is a copy of the output from the EDS unit. The second set lists the data after renormalizing to reflect the presence of crystalline water (H_2O^+ set at 20.93 wt. %, theoretical water content in gypsum).

Vial No. 7, Kolbeinsey Ridge

Three samples were selected from vial no. 7. Under the binocular microscope Sample A is an aggregate of yellowish- and reddish-brown crystals. The SEM overview shot of sample A is in Figure 3a. The areas that are charging (bright areas) in Figure 3a are near-white in color under the binocular scope. Much of the aggregate is composed of pyrite crystals (Figure 3b,d-f; Table 4). Occasional growths of barite crystals are scattered throughout the pyrite (Figure 3b,c; Table 5). Quantitative analysis of the barite crystal marked in Figure 3b shows that the crystal contains approximately 10 percent by weight (wt. %) Sr. Examination of the pyrite crystal surfaces at higher magnification shows that etching by oxidation has occurred (Figure 3g). Some places on the surface were protected from attack by smaller particles that have fallen off. Oxidation of the iron in the pyrite would explain the yellowish and reddish-brown color noticed under the binocular scope. The description submitted with vial no. 7 indicates that it was a "wet vial". Oxidation could have occurred in the vial. The whitish material (the area charging in Figure 3a) and the smaller particles scattered on the surface of the pyrite in Figure 3g is smectite (See the description of sample C below).

Sample B consists of a number of smaller grains and aggregates that were selectively picked from vial No. 7 in an attempt to isolate the dark reddish-brown material mentioned in sample A (Figure 3h). SEM/EDS examination of the reddish-brown areas showed that it is an iron oxide coating. One area examined (Figure 3i) is composed of smectite coated with iron oxide that probably is the result of pyrite oxidation. EDS analyses of this sample were not recorded. Other components present include particles of silica and halite.

Under the binocular microscope, Sample C appears to be a consolidated, fine-grained material, green/gray in color. An SEM micrograph of Sample C is shown in Figure 3j. The texture of the material (Figure 3k,l) resembles the texture of smectite (Welton, 1984). EDS analysis is shown in Figure 3m and Table 6. Additional material was removed from the vial and prepared for analysis with the x-ray diffractometer. Diffraction peaks characteristic of smectite are present. Diffraction peaks for pyrite, barite, and gypsum are also present.

Figure 3: Three samples from Kolbeinsey Ridge, vial no. 7; SEM micrographs and EDS spectra.

Sample A:

a - Aggregate of pyrite crystals; areas that are charging (bright areas) are smectite.

b - Barite crystals (tabular plates) growing on pyrite; pyrite covered with halite (center of picture) and particles of smectite.
c - EDS spectrum of location marked (with a dot) on barite plate in 3b; quantitative results in Table 5.
d - Pyrite crystals lightly covered with particles of smectite.
e - EDS spectrum of a pyrite crystal in sample A; quantitative results in Table 4.
f - Pyrite crystals covered with scattered particles of smectite.
g - Close-up of oxidized surface of pyrite crystal; smectite particles on pyrite; spots protected from oxidation marked with arrows.

Sample B:

h - Selected grains from the vial containing the dark reddish-brown (iron oxide) material; iron oxide is circled.
i - Iron oxide coating on smectite; pyrite crystals (P) lower right.

Sample C:

j - Sample C, fine-grained aggregate, smectite.
k - Texture of smectite aggregate.
l - Higher magnification view of an area in right center of 3k.
m - EDS spectrum of aggregate; quantitative results in Table 6.

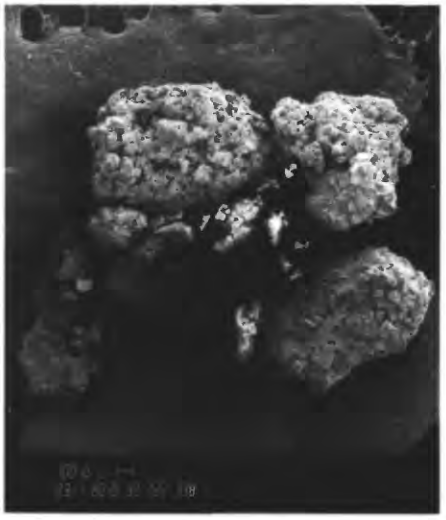

a

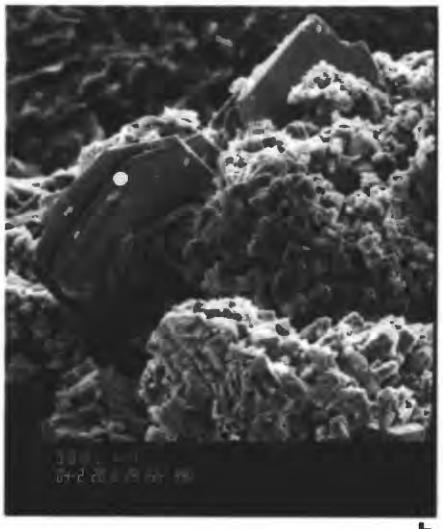

b

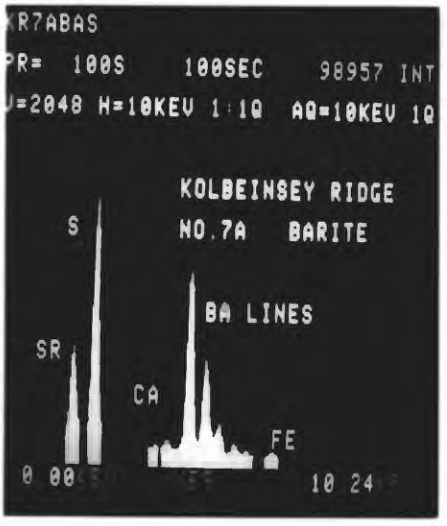

c

d

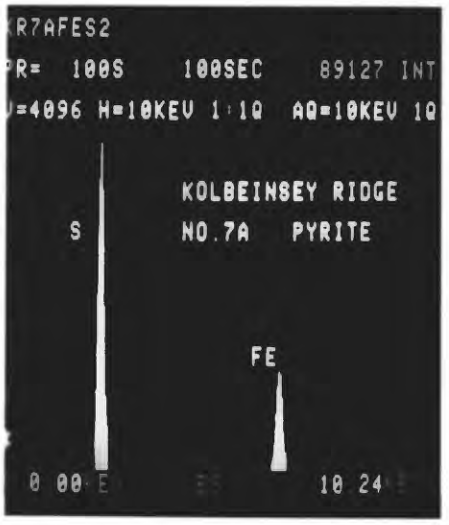

e

Figure 3

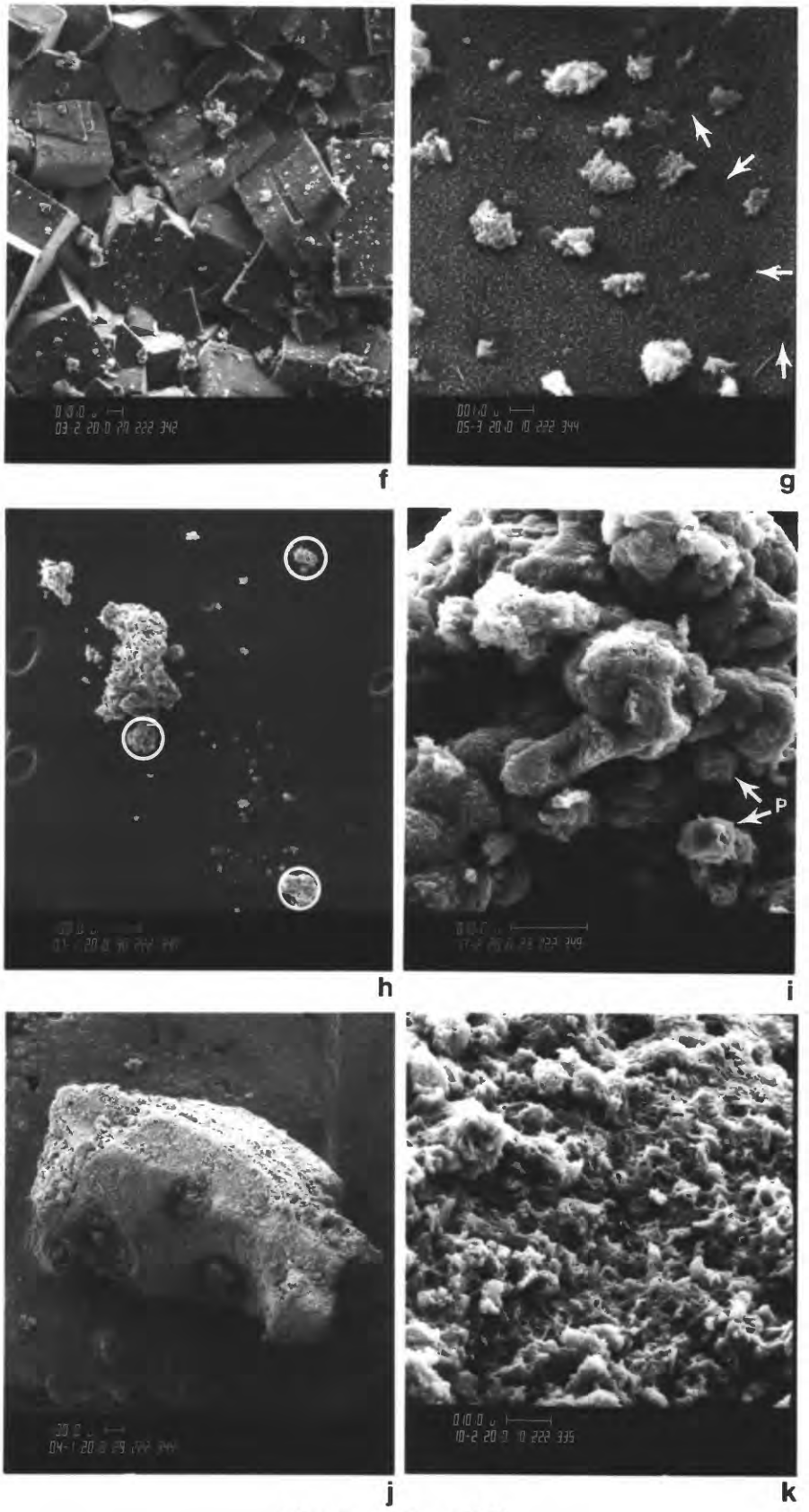

Figure 3 (cont'd)

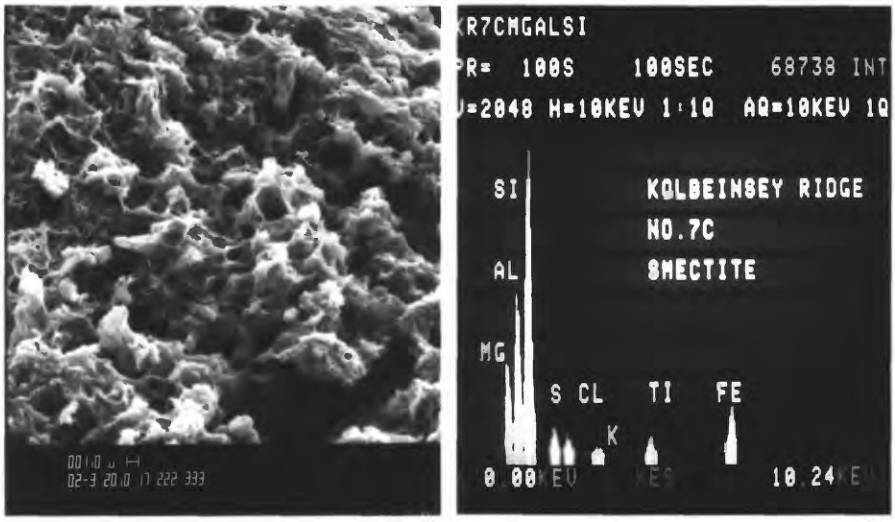

l m

Figure 3 (cont'd)

EDS output:

Element	Wt. %	At. %	Precision 2 Sigma	Theoretical Composition of Pyrite (Wt. %)
S	53.66	66.85	0.46	53.45
Fe	46.34	33.15	0.67	46.55
Total	100.00	100.00		100.00

Table 4. Kolbeinsey Ridge, vial no. 7; analysis of a pyrite crystal in Sample A (output from EDS unit). The theoretical composition of pyrite is listed.

EDS output:

Element	Wt. %	Precision 2 Sigma	El. Oxide	Wt. %
S	15.00	0.34	SO_3	37.44
Ca	0.33	0.11	CaO	0.47
Fe	1.20	0.20	Fe_2O_3	1.72
Sr	9.82	0.49	SrO	11.61
Ba	43.67	0.93	BaO	48.76
O *	29.98			
Total	100.00			100.00

Data after removing Fe and S attributed to pyrite:

Element	Wt. %	At. %	El. Oxide	Wt. %
S	14.36	16.49	SO_3	35.86
Ca	0.36	0.33	CaO	0.50
Sr	10.35	4.35	SrO	12.24
Ba	46.04	12.34	BaO	51.40
O *	28.89	66.49		
Total	100.00	100.00		100.00

* Determined by stoichiometry

Table 5. Kolbeinsey Ridge, vial no. 7; analysis of a barite plate in Sample A (marked in Figure 3b). The first set of data is a copy of the output from the EDS unit. The second set lists the data after mathematically removing the Fe (Fe_2O_3) and a corresponding amount of S (SO_3) attributed to pyrite.

EDS output:

Element	Wt. %	Precision 2 Sigma	El. Oxide	Wt. %
Mg	9.61	0.41	MgO	15.93
Al	11.57	0.37	Al_2O_3	21.87
Si	18.80	0.36	SiO_2	40.22
S	1.49	0.16	SO_3	3.72
Cl	0.93	0.12	Cl	0.93
K	0.56	0.14	K_2O	0.67
Ti	1.86	0.19	TiO_2	3.10
Fe	9.48	0.39	Fe_2O_3	13.56
O *	45.70			
Total	100.00			100.00

* Determined by stoichiometry

Table 6. Kolbeinsey Ridge, vial no. 7; analysis of fine-grained aggregate of smectite in Sample C. Since OH in the smectite cannot be measured by the EDS detector, the values listed are too high because of the normalization technique used. Element or element oxide ratios derived from the values listed are valid.

Vial A, Reykjanes Ridge

There was only one large grain in the vial. Under the reflected light of the binocular microscope, the grain contained alternating light (white) and dark (black-brown) layers of fine-grained material. Under the binocular microscope, the dark areas in the SEM photo (Figure 4a) are light areas and the light areas in the photo are dark. SEM/EDS examination showed that the grain is a piece of manganese oxide crust (Figure 4a-l; Table 7). The banding effect seen in Figure 4a-c is due to the presence of halite (the dark zones). Perhaps the halite leached out of the more porous layers of the manganese crust as the sample dried.

There are a number of small cavities on the broken surface of the crust (Figure 4b-f) that resemble cavities created by boring organisms. We have seen evidence of such borings in ferromanganese crusts from the Florida escarpment (A. C. Neumann, Univ. of North Carolina, unpublished data, 1988). Inside some of the cavities are spherical growths that appear to be organic (Figure 4d-f). EDS analysis of these spheres (not documented in the photos) showed the broad continuum hump typical of organic material with only a small S peak and a peak for Mn. The Mn peak is coming from the oxide crust on which the spheres are growing and the S is contained in the organic material.

The manganese oxide material is fairly pure as there is very little iron oxide phase associated with it (Figure 4h,j; Table 7). SEM examination of growth surfaces (Figure 4k-l) shows crystalline forms resembling todorokite. The results of EDS analysis (Table 7) are similar to data reported for todorokites and birnessites by Burns and Burns (1979).

The output from the EDS unit (Table 7) has been normalized to 100 percent. The values are too high because the EDS detector cannot measure H_2O present as crystalline water. The EDS output data has been renormalized to include crystalline water (H_2O^+) and a correction for Cl content. H_2O^+ is calculated from the following empirically determined relationship (Manheim and Lane-Bostwick, 1989).

$$H_2O^+ = (MnO_2 + Fe_2O_3)/7$$

where

MnO_2 and Fe_2O_3 are measured components of the manganese oxide crust.

A correction for Cl content is necessary in the renormalization process because a portion of some of the elements listed in the table are present as chlorides. For example, part of the Na may be present as NaCl. As the EDS

technique cannot determine which elements are present as chlorides, the oxide data (O, calculated by stoichiometry) are allowed to total slightly above 100 percent. Oxygen listed in the element column has been corrected for Cl content and the column totals to 100 percent.

Figure 4: Manganese crust fragment from Reykjanes Ridge, vial A; SEM micrographs and EDS spectra.

a - Fragment of "banded" manganese oxide crust; dark areas covered with halite; outer growth surface located inside box.
b - Fractured surface of manganese oxide crust; shows banding, dark layers are halite and light layers are manganese oxide; cavities in crust across center of micrograph.
c - Enlargement of fractured surface; shows cavities; halite (dark zones) across center and bottom of photo.
d - Cavities in manganese oxide crust; Sulfur-bearing spherical growths in dark cavity on right side; halite coating across bottom of picture.
e - Sulfur-bearing spherical growth in urn shaped cavity in 4c (bottom right).
f - Sulfur-bearing spherical growth in cavity.
g - Enlargement of area circled at top of 4c; texture of fractured surface.
h - EDS spectrum of manganese oxide near 4g; quantitative results in Table 7, Analysis 1.
i - Enlargement of area circled at bottom of 4c; texture of fractured surface.
j - EDS spectrum of manganese oxide near 4i; quantitative results in Table 7, Analysis 2.
k - Growth surface on manganese oxide crust (inside box in 4a); crystalline forms resemble todorokite.
l - Enlargement of an area (left center) in 4k; growth surface.

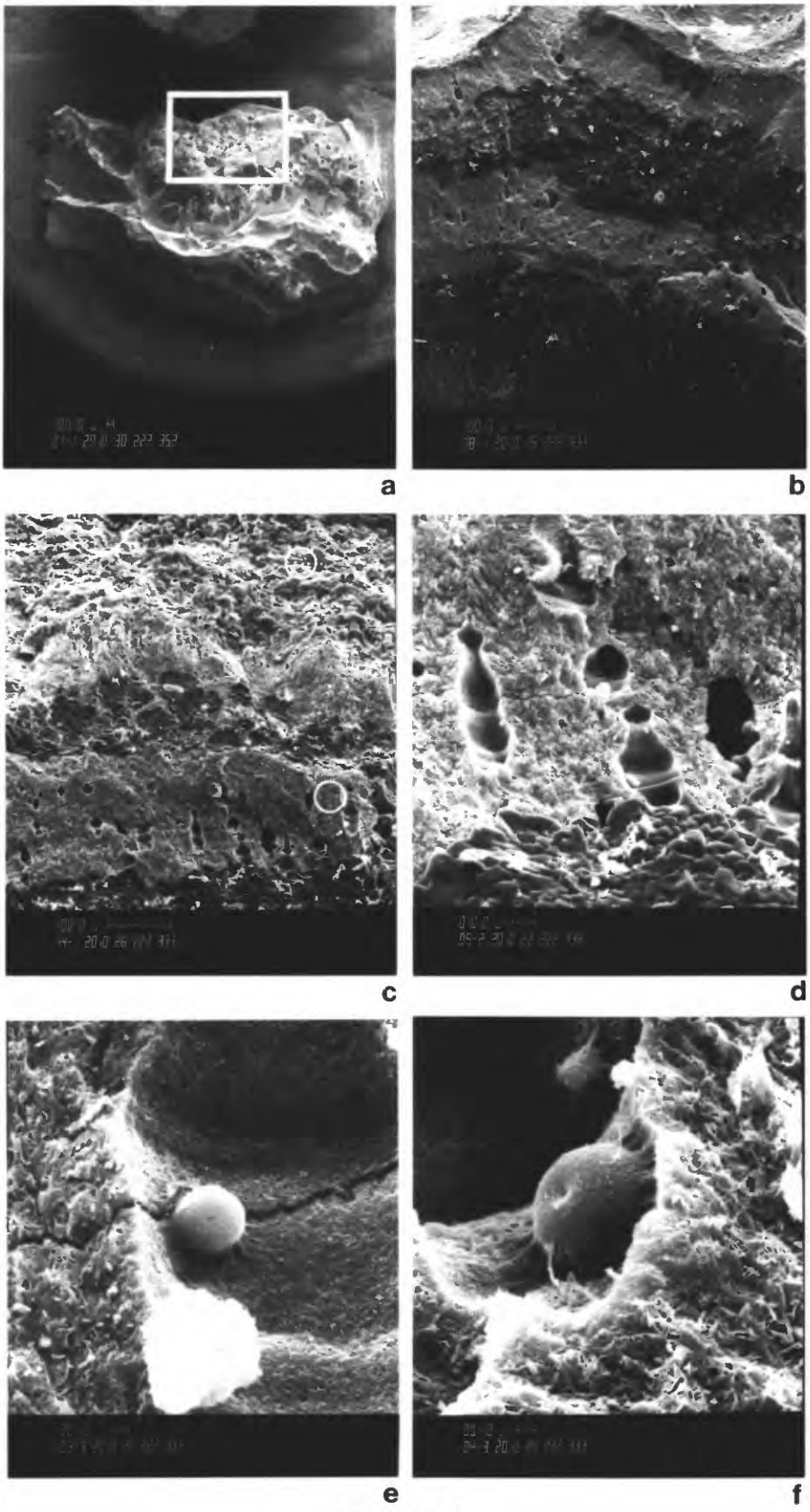

Figure 4

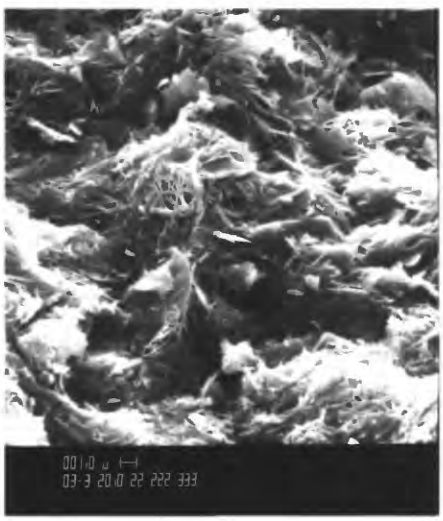

g

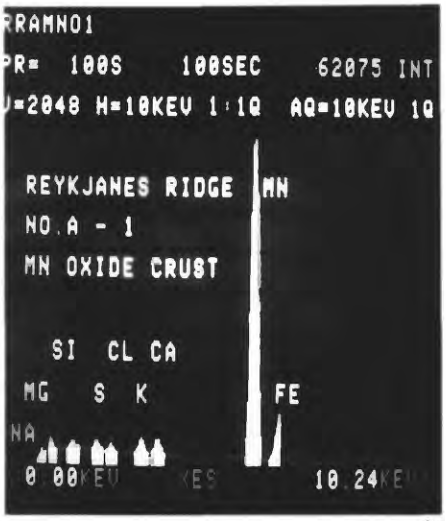

h

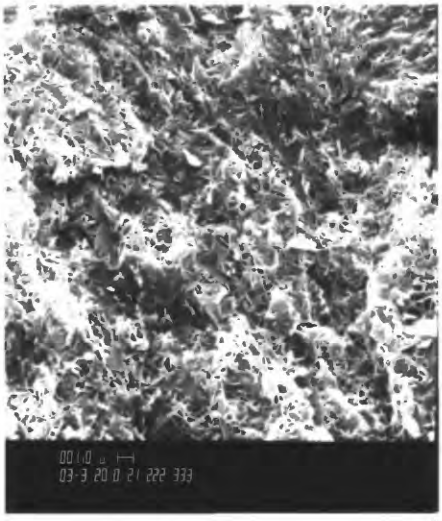

i

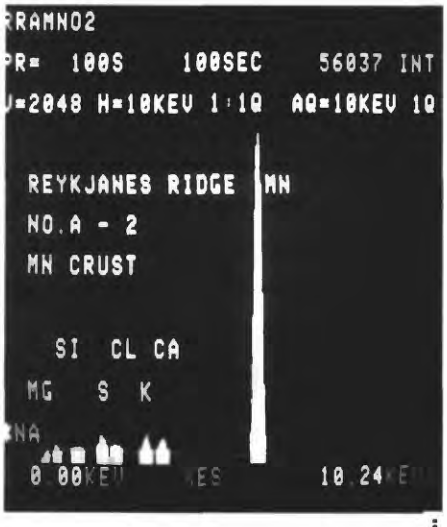

j

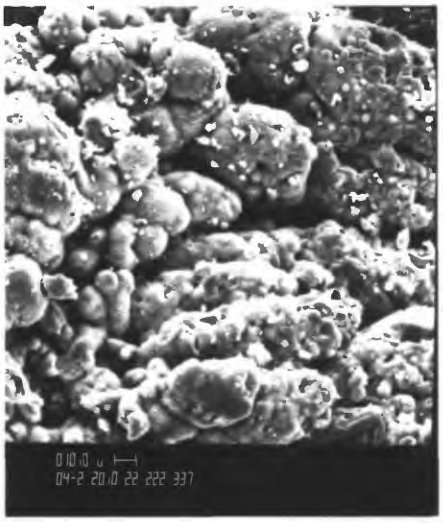

k

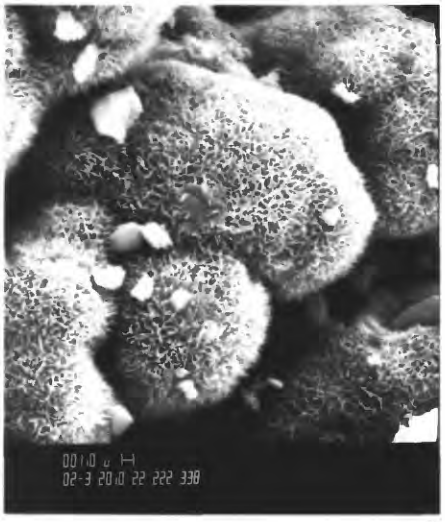

l

Figure 4 (cont'd)

Analysis 1:

Element	Wt. %	Precision 2 Sigma	El. Oxide	Wt. %
Na	2.42	0.47	Na_2O	3.26
Mg	1.78	0.24	MgO	2.95
Si	0.48	0.12	SiO_2	1.03
S	0.57	0.11	SO_3	1.42
Cl	0.42	0.11	Cl	0.42
K	1.09	0.12	K_2O	1.31
Ca	1.18	0.12	CaO	1.66
Mn	55.34	0.65	MnO_2	87.57
Fe	0.27	0.29	Fe_2O_3	0.38
O *	36.46			
Total	100.00			100.00

Analysis 2:

Element	Wt. %	Precision 2 Sigma	El. Oxide	Wt. %
Na	2.60	0.40	Na_2O	3.50
Mg	1.27	0.20	MgO	2.11
Si	0.22	0.10	SiO_2	0.47
S	0.82	0.11	SO_3	2.05
Cl	0.29	0.10	Cl	0.29
K	1.16	0.11	K_2O	1.40
Ca	1.03	0.11	CaO	1.44
Mn	56.08	0.56	MnO_2	88.74
Fe	BDL		Fe_2O_3	BDL
O *	36.53			
Total	100.00			100.08

* Determined by stoichiometry

BDL = below detection limit (0.1 element wt. %)

Table 7. Reykjanes Ridge, vial A; analysis of manganese oxide crust fragment near Figure 4g (Analysis 1) and Figure 4i (Analysis 2) - output from EDS unit. Since the data was normalized to 100 percent, the values are too high because the EDS system cannot detect the crystalline water. Concentration ratios derived from the data listed are valid. Table 7 continued on next page.

Analysis 1:

Element	Wt. %	El. Oxide	Wt. %
H #	1.25	H_2O^+ #	11.17
Na	2.17	Na_2O	2.92
Mg	1.58	MgO	2.62
Si	0.43	SiO_2	0.91
S	0.50	SO_3	1.26
Cl	0.37	Cl	0.37
K	0.97	K_2O	1.17
Ca	1.05	CaO	1.47
Mn	49.19	MnO_2	77.85
Fe	0.24	Fe_2O_3	0.34
O *	42.25		
Total	100.00		100.08

Analysis 2:

Element	Wt. %	El. Oxide	Wt. %
H #	1.26	H_2O^+ #	11.26
Na	2.32	Na_2O	3.13
Mg	1.13	MgO	1.87
Si	0.20	SiO_2	0.42
S	0.73	SO_3	1.82
Cl	0.26	Cl	0.26
K	1.03	K_2O	1.24
Ca	0.91	CaO	1.28
Mn	49.78	MnO_2	78.78
Fe	BDL	Fe_2O_3	BDL
O *	42.38		
Total	100.00		100.06

Calculated H_2O^+ (and H); see text

BDL = below detection limit (0.1 element wt. %)

* Determined by stoichiometry, corrected for Cl

Table 7 (continued). Reykjanes Ridge, vial A; analysis of manganese oxide crust fragment near Figure 4g (Analysis 1) and Figure 4i (Analysis 2). Data renormalized to include calculated crystalline water (H_2O^+) and a correction for Cl content.

Vial D, Reykjanes Ridge

Two samples were mounted for SEM/EDS analysis: one of the larger grains in the vial and some of the powder that was coating it. The grain is a fragment of manganese oxide crust (Figure 5a). Under the optical scope, the grain is black-brown in color and shows banding along fractured surfaces. The sample was oriented on the SEM stub so the banding could be examined. The banding effect is created by the radial, layered pattern of manganese mineral growth (Figure 5b). The growth surfaces show crystalline forms that resemble todorokite (Figure 5c). Holes in the outer surface were created by boring organisms (Figure 5d). EDS analyses of three small areas (Figure 5e-g; Table 8) show that the crust is almost pure manganese mineral growth with little or no associated iron oxide phase. The locations of the analyses are marked in Figure 5a. As in the sample from vial A, The output data from the EDS unit (Table 8) are too high because the EDS detector cannot measure water in the structure. The EDS output data have been renormalized to include crystalline water and a correction for Cl content (see the discussion of the crust fragment from vial A). The data in Table 8 are also similar to data published in the literature for todorokite and birnessite (Burns and Burns, 1979). Compared to the results in Table 7 for the crust fragment in vial A, this fragment has on average more Ca, less K, and less Mg. After completion of the SEM/EDS analysis, the crust fragment was ground into a powder and run on the x-ray diffraction spectrometer. X-ray lines characteristic of both todorokite (9.5 - 9.8 A and 4.8 - 4.9 A) and birnessite (7.0 - 7.3 A and 3.5 - 3.6 A) are present. However, the birnessite may not be an original component of the manganese crust. It can form as an alteration product as todorokite de-waters during storage or perhaps even during exposure to the x-ray beam in the diffractometer (R. G. Burns, oral commun., 1989).

The second sample, the black-brown powder coating the crust fragment, is manganese oxide (Figure 5h,i). The output from the EDS unit and renormalized data that include crystalline water and a correction for Cl content are presented in Table 9. No iron phase is present. There is more Cl in the powder than in the crust fragment from vial D, and also a small amount of Cu. The chemistry is similar to the todorokite and birnessite data previously mentioned.

Figure 5: Manganese crust fragment and black-brown powder from Reykjanes Ridge, vial D; SEM micrographs and EDS spectra.

Fragment:

a - Fragment of manganese oxide crust; fracture surface showing growth layering; locations of analyses in Table 8 marked on photo.
b - Cross section of crust roughly normal to growth surface; shows radial

growth pattern and layering; growth surface across top of picture.

c - Growth surface on manganese oxide crust, crystalline forms resemble todorokite.

d - Holes created by boring organisms on outer surface of manganese crust.

e - EDS spectrum of manganese oxide; results in Table 8, Analysis 1; analysis marked in 5a.

f - EDS spectrum of manganese oxide, results in Table 8, Analysis 2; analysis marked in 5a.

g - EDS spectrum of manganese oxide, results in Table 8, Analysis 3; analysis marked in 5a.

Powder:

h - Black-brown powder coating manganese crust fragment.

i - EDS spectrum of manganese oxide powder; results in Table 9.

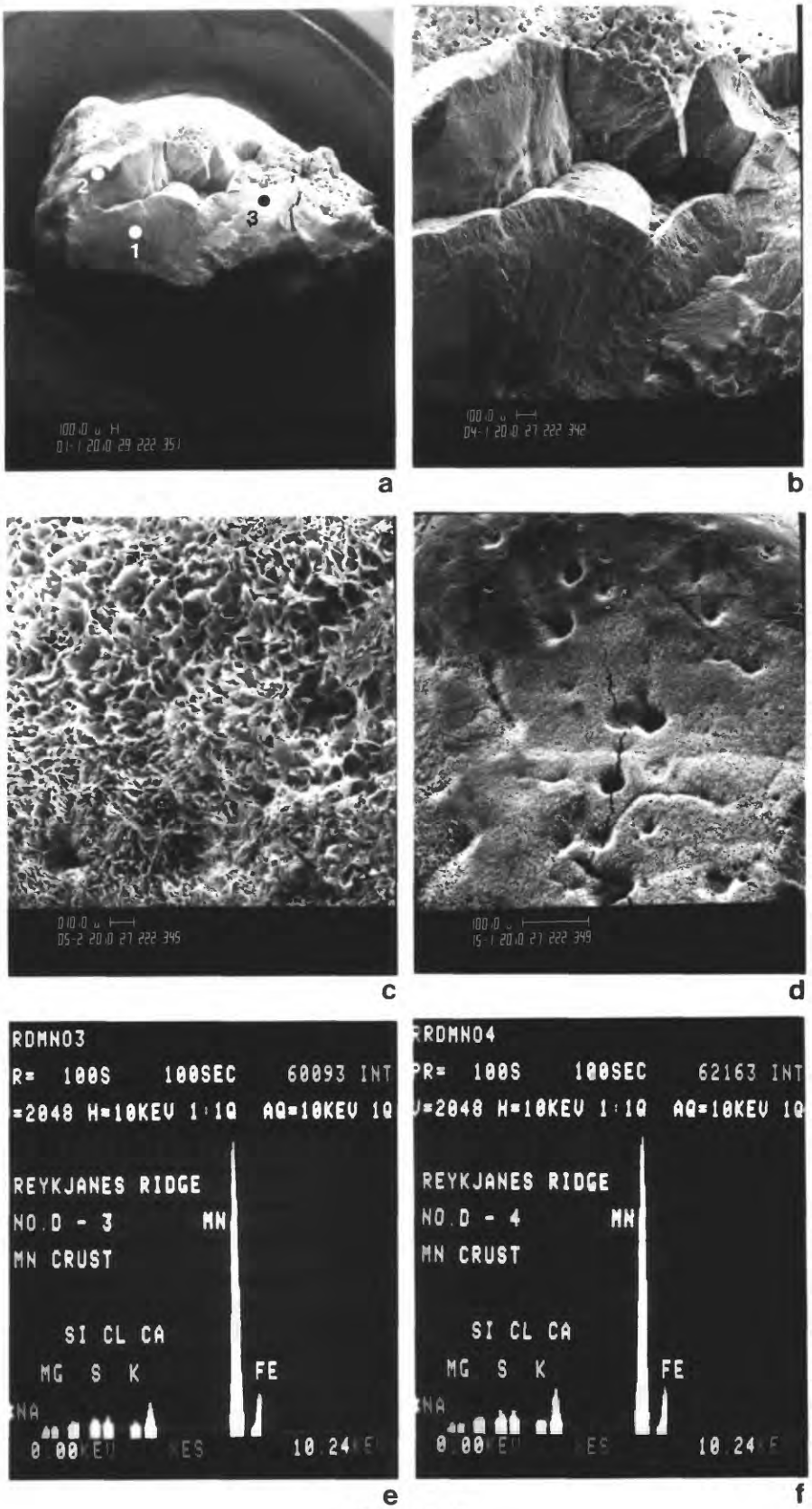
2
3
1
a
b
c
d
RDMNO3
R= 100S 100SEC 60093 INT
=2048 H=10KEV 1:1Q AQ=10KEV 1Q
REYKJANES RIDGE
NO.D - 3
MN
MN CRUST
SI CL CA
MG S K
FE
RDMNO4
REYKJANES RIDGE
NO.D - 4
MN
MN CRUST
SI CL CA
MG S K
FE
e
f

Figure 5

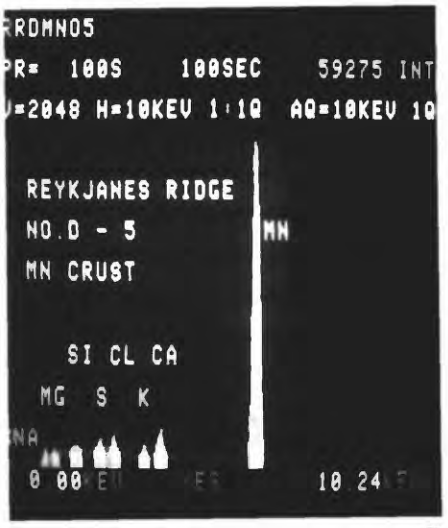

g

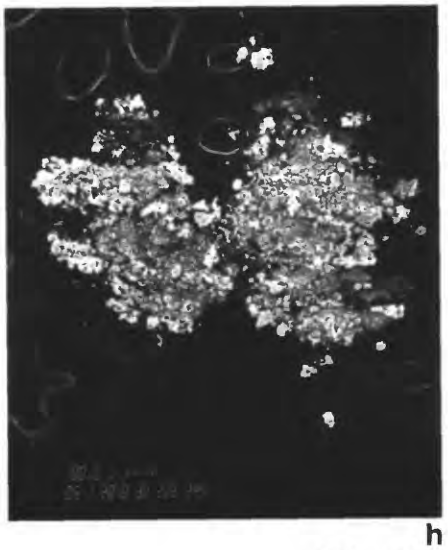

h

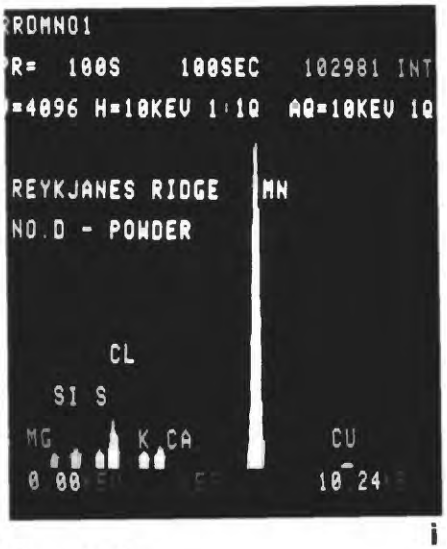

i

Figure 5 (cont'd)

Analysis 1:

El.	Wt. %	Prec. 2 Sigma	El. Ox.	Wt. %
Na	3.81	0.44	Na_2O	5.14
Mg	0.65	0.18	MgO	1.08
Si	0.42	0.10	SiO_2	0.89
S	0.70	0.09	SO_3	1.75
Cl	0.78	0.11	Cl	0.78
K	0.48	0.10	K_2O	0.58
Ca	2.29	0.12	CaO	3.21
Mn	54.46	0.54	MnO_2	86.17
Fe	0.28	0.27	Fe_2O_3	0.39
O *	36.13			
Tot.	100.00			100.00

Analysis 2:

El.	Wt. %	Prec. 2 Sigma	El. Ox.	Wt. %
Na	2.47	0.36	Na_2O	3.33
Mg	0.40	0.16	MgO	0.66
Si	0.33	0.10	SiO_2	0.70
S	0.73	0.09	SO_3	1.83
Cl	0.87	0.11	Cl	0.87
K	0.31	0.09	K_2O	0.37
Ca	3.11	0.13	CaO	4.35
Mn	55.19	0.55	MnO_2	87.34
Fe	0.38	0.27	Fe_2O_3	0.54
O *	36.21			
Tot.	100.00			100.00

Analysis 3:

El.	Wt. %	Prec. 2 Sigma	El. Ox.	Wt. %
Na	4.23	0.48	Na_2O	5.71
Mg	0.98	0.21	MgO	1.62
Si	0.49	0.11	SiO_2	1.06
S	0.78	0.09	SO_3	1.95
Cl	1.04	0.11	Cl	1.04
K	0.61	0.10	K_2O	0.73
Ca	1.84	0.12	CaO	2.58
Mn	53.92	0.54	MnO_2	85.32
Fe	BDL		Fe_2O_3	BDL
O *	36.11			
Tot.	100.00			100.00

BDL = below detection limit (0.1 element wt. %)

* Determined by stoichiometry

Table 8. Reykjanes Ridge, vial D; analyses of manganese oxide crust fragment, output from EDS unit. Location of analyses marked in Figure 5a. Since the data was normalized to 100 percent, the values are too high because the EDS system cannot detect the crystalline water. The concentration ratios derived from the values listed are valid. Table 8 continued on next page.

Analysis 1:

Element	Wt. %	El. Oxide	Wt. %
H #	1.23	H_2O^+ #	11.02
Na	3.42	Na_2O	4.61
Mg	0.58	MgO	0.96
Si	0.37	SiO_2	0.80
S	0.62	SO_3	1.56
Cl	0.69	Cl	0.69
K	0.43	K_2O	0.52
Ca	2.04	CaO	2.85
Mn	48.52	MnO_2	76.79
Fe	0.25	Fe_2O_3	0.36
O *	41.83		
Total	100.00		100.16

Analysis 2:

Element	Wt. %	El. Oxide	Wt. %
H #	1.25	H_2O^+ #	11.17
Na	2.21	Na_2O	2.98
Mg	0.36	MgO	0.59
Si	0.29	SiO_2	0.63
S	0.65	SO_3	1.62
Cl	0.77	Cl	0.77
K	0.27	K_2O	0.33
Ca	2.77	CaO	3.87
Mn	49.12	MnO_2	77.73
Fe	0.34	Fe_2O_3	0.48
O *	41.98		
Total	100.00		100.17

Analysis 3:

Element	Wt. %	El. Oxide	Wt. %
H #	1.22	H_2O^+ #	10.88
Na	3.81	Na_2O	5.13
Mg	0.87	MgO	1.45
Si	0.44	SiO_2	0.94
S	0.70	SO_3	1.74
Cl	0.93	Cl	0.93
K	0.55	K_2O	0.66
Ca	1.64	CaO	2.30
Mn	48.14	MnO_2	76.18
Fe	BDL	Fe_2O_3	BDL
O *	41.71		
Total	100.00		100.21

Calculated H_2O^+ (and H); see text

BDL = below detection limit (0.1 element wt. %)

* Determined by stoichiometry, corrected for Cl

Table 8 (continued). Reykjanes Ridge, vial D; analyses of manganese oxide crust fragment, data renormalized to include calculated crystalline water (H_2O^+) and a correction for Cl content. Location of analyses marked in Figure 5a.

EDS output:

Element	Wt. %	Precision 2 Sigma	El. Oxide	Wt. %
Na	BDL		Na_2O	BDL
Mg	0.88	0.19	MgO	1.45
Si	0.47	0.11	SiO_2	1.00
S	0.20	0.09	SO_3	0.50
Cl	3.03	0.13	Cl	3.03
K	0.65	0.11	K_2O	0.78
Ca	1.15	0.11	CaO	1.61
Mn	57.59	0.58	MnO_2	91.14
Fe	BDL		Fe_2O_3	BDL
Cu	0.38	0.19	CuO	0.48
O *	35.65			
Total	100.00			100.00

Data re-normalized to include crystalline water; corrected for Cl:

Element	Wt. %	El. Oxide	Wt. %
H #	1.30	H_2O^+ #	11.59
Na	BDL	Na_2O	BDL
Mg	0.78	MgO	1.30
Si	0.42	SiO_2	0.89
S	0.18	SO_3	0.44
Cl	2.70	Cl	2.70
K	0.58	K_2O	0.70
Ca	1.02	CaO	1.43
Mn	51.27	MnO_2	81.14
Fe	BDL	Fe_2O_3	BDL
Cu	0.34	CuO	0.42
O **	41.42		
Total	100.00		100.61

Calculated H_2O^+ (and H); see text

BDL = below detection limit (0.5 wt.% Na; 0.1 wt.% Fe)

* Determined by stoichiometry

** Determined by stoichiometry, corrected for Cl

Table 9. Reykjanes Ridge, vial D; analysis of manganese oxide powder. The first set of data is a copy of the output from the EDS unit (values too high, concentration ratios valid - see text). The second set lists the data after renormalizing to include calculated crystalline water (H_2O^+) and a correction for Cl content.

IV SUMMARY

As a result of magmatism and volcanic activity, super-heated waters rise under pressure along fissures in the earth's crust and along sedimentary boundaries to the ocean floor. These hydrothermal fluids contain dissolved metals and hydrogen sulfide originating from the magma, the crustal material, and the sediments. As they approach and exit the sea floor, the fluids undergo a decrease in pressure and temperature and, as they mix with sea water, an increase in pH and dissolved oxygen. At the sea floor, precipitation occurs in the form of metallic sulfides, sulfates, silicates, and oxide/hydroxides. The chemical components necessary for mineralization are supplied by the discharging hydrothermal fluids and by sea water.

Most of the mineral phases observed in this study appear to be precipitated either directly from discharging hydrothermal fluids at the sea floor or by post-depositional, diagenetic reactions involving hydrothermally derived elements or oxides.

Kolbeinsey Ridge Samples

The mineral phases observed in the Kolbeinsey Ridge samples can be divided into three categories:

Hydrothermal	Possible Artifact	Artifact
Pyrite	Gypsum	Halite
Silica Amorphous		Glauberite or similar Na-Ca sulphate
Smectite		
Barite High-Sr		
Gypsum		

The pyrite documented in this study precipitated when venting fluids containing dissolved Fe and H_2S mixed with sea water and were rapidly cooled. The pyrite is stoichiometrically pure FeS_2.

Silica, a major component in venting hydrothermal fluids, can form as botryoidal growths on other mineral assemblages. For example, Haymond and Kastner (1981) have reported amorphous silica globules on metallic sulfide surfaces.

The silica phase reported in this study exhibits the globular, botryoidal growth pattern and is coating pyrite.

Iron-rich smectite is commonly found in a hydrothermal setting. It can precipitate directly from the discharging fluids by reactions of silica with Fe, or it can form diagenetically from hydrothermally derived precipitates (silica and iron hydroxides) on the sea floor and in the water column (Bonatti, 1983).

Barite is also a common mineral in marine hydrothermal deposits, usually attributable to the interaction of interstitial or discharging solutions containing elevated concentrations of barium (and depleted sulfate) with sulfate from sea water or oxidized sulfides. The barite in our studied samples contains 4.3 atomic percent Sr (Table 5) which is significantly higher than barites formed in ambient seawater or sea-floor conditions. Following Church (1979) we conclude that the elevated Sr content in this barite may be attributable to the high temperature, rather than a higher Sr concentration, of the discharging solutions.

Gypsum precipitates as the hydrothermal fluids mix with sea water. The chemical components necessary for its formation may be derived from a number of sources: Ca may be carried in the fluids (Edmond, 1982), and it is also a component in sea water. Sulfate is a component in sea water and also is an oxidation product of H_2S or metallic sulfides in contact with sea water. The gypsum documented in this study probably precipitated in place on the sea floor because gypsum is known to be a major component in other samples from the same area (J. Olafsson and others, manuscript in preparation, 1989). However, we recognize that gypsum is an evaporite mineral and it could be an artifact formed as sea water in the sample dried.

Halite and glauberite, the Na - Ca sulfate mineral, are clearly artifacts of sample drying.

Reykjanes Ridge Samples

The major phase observed in the Reykjanes Ridge samples is MnO_2 or Todorokite. The MnO_2 phase is clearly hydrothermal, as demonstrated by the extreme Mn/Fe ratios of 70 or more. No Co, Ni, or other metals characteristic of slowly accumulating crusts of hydrogenous origin are detected in the manganese crust fragments. The manganese powder sample showed .42 oxide percent Cu. However it is also clearly of hydrothermal origin because it showed extreme Mn/Fe ratios (>100). Cu-enriched manganese oxides of hydrothermal origin have recently been identified in samples collected from the East Pacific Rise near 7^0N and 14^0N (Stouff and Boulegue, 1989). The manganese mineral has a bladed habit under magnifications greater than 500 times and resembles published descriptions for todorokite (Burns and Burns, 1979). It is similar in form to reported manganese oxide hydrothermal precipitates also recovered from the Atlantic Ocean (Thompson and others, 1985; 1988; Lalou and others, 1988). The data in Tables 7, 8, and 9 have

been renormalized to include calculated crystalline water (H_2O^+) after Manheim and Lane-Bostwick (1989).

ACKNOWLEDGEMENTS

We thank Lawrence J. Poppe, U.S. Geological Survey, for performing the x-ray diffraction analysis of selected samples. We are also indebted to Page C. Valentine, U.S. Geological Survey, and Susumu Honjo, Woods Hole Oceanographic Institution, for their thoughtful suggestions during the preparation of the final manuscript.

REFERENCES

Bonnatti, E., 1983, Hydrothermal metal deposits from the oceanic rifts: a classification, in Rona, P. A., and others, eds., Hydrothermal processes at seafloor spreading centers; v. 12 of Series IV, Marine Sciences: New York, Plenum, p. 491-502.

Burns, R. G., and Burns, V. M., 1979, Manganese oxides, in Burns, R. G., ed., Marine minerals, v. 6 of Reviews in mineralogy: Washington, D. C., Mineralogical Society of America, p. 1-46.

Church, T. M., 1979, Marine barite, in Burns, R. G., ed., Marine minerals, v. 6 of Reviews in mineralogy: Washington, D. C., Mineralogical Society of America, p. 175-210.

Colby, J. W., 1968, Quantitative microprobe analysis of thin insulating films, in Newkirk, J. B., and others, eds., Advances in x-ray analysis: New York, Plenum, v. 11, p. 289-305.

Duffield, W. A., 1978, Vesicularity of basalt erupted at Reykjanes Ridge crest: Nature, v. 254, p. 298-301.

Edmond, J. M., 1982, The chemistry of ridge crest hot springs: Marine Technology Society Journal, v. 16, no. 3, p. 23-25.

Einarsson, P., 1986, Seismicity along the eastern margin of the North Atlantic Plate, in Vogt, P. R., and Tucholke, B. E., eds., The Western North Atlantic, v. M: The Geology of North America: Geological Society of America, p. 69-86.

Haymond, R. M., and Kastner, M., 1981, Hot spring deposits on the East Pacific Rise at 21°N: preliminary description of mineralogy and genesis: Earth and Planetary Science Letters, v. 53, p. 363-381.

Lalou, C. E., Brichet, E., and Thompson, G., 1988, Radionuclide gradients in two Mn oxide deposits from the Mid-Atlantic Ridge: possible influence of a hydrothermal plume: Canadian Mineralogist, v. 26, p. 713-720.

Manheim, F. T., and Lane-Bostwick, C. M., editors, 1989, Chemical composition of ferromanganese crusts in the world ocean: a review and comprehensive data base: U.S. Geological Survey Open-File Report 89-020, 200 p.

Saemundsson, K., 1986, Subaerial volcanism in the western North Atlantic, in Vogt, P. R., and Tucholke, B. E., eds., The Western North Atlantic, v. M: The Geology of North America: Geological Society of America, p. 99-116.

Stouff, P., and Boulegue, J., 1989, Geochemistry and crystallochemistry of oceanic hydrothermal manganese oxyhydroxides showing manganese-copper association: Geochim. Cosmochim. Acta, v. 53, no. 4, p. 833-843.

Thompson, G., Mottl, M. J., and Rona, P. A., 1985, Morphology, mineralogy and chemistry of hydrothermal deposits from the TAG area, 26^{0}N Mid-Atlantic Ridge: Chemical Geology, v. 49, p. 243-257.

Thompson, G., Humphris, S. E., Schroder, B., and Sulsanowska, M., 1988, Active vents and massive sulfides at 26^{0}N (TAG) and 23^{0}N (Snakepit) on the Mid-Atlantic Ridge: Canadian Mineralogist, v. 26, p. 697-711.